Microscopic evidence for magnetic-phase coexistence in the intermetallic compound Nd$_7$Rh$_3$

S. Rayaprol,[1,*] V. Siruguri,[1] A. Hoser,[2] C. Ritter,[3] and E. V. Sampathkumaran[4]

[1]*UGC-DAE Consortium for Scientific Research - Mumbai Centre, R5 Shed, Trombay, Mumbai 400085, India*

[2]*Helmholtz-Zentrum Berlin für Materialien und Energie, D-14109 Berlin, Germany*

[3]*Institut Laue-Langevin, BP 156, F-38042 Grenoble, France*

[4]*Tata Institute of Fundamental Research, Homi Bhabha Road, Colaba, Mumbai 400005, India*

The intermetallic compound Nd$_7$Rh$_3$, which shows two magnetic transitions, one at 32 K and another around 16 K, has been known to exhibit a magnetic-field induced first-order magnetic phase transition (FOPT) at low temperatures. Using neutron diffraction we tracked the evolution of the magnetic features as a function of temperature and external magnetic field across the two transition temperatures. We provide evidence for the existence of both antiferromagnetism and ferromagnetism below 20 K. Notably the results reveal concrete evidence for the partial persistence of the high-field magnetic state at 2 K after cycling through the magnetic-field-induced magnetic transition, thereby offering microscopic evidence for magnetic coexistence phenomenon in this intermetallic compound.

I. INTRODUCTION

Electronic phase separation (EPS) phenomena have been observed following field cycling across first-order metal-insulator transitions driven by temperature (T) or magnetic field (H) [1,2]. EPS has been extensively studied in giant magnetoresistive manganites. It is believed that EPS, and the resulting percolative conduction, is a more general phenomenon in materials which exhibit disorder-influenced first-order phase transitions (FOPT) [1,2]. However, similar studies on stoichiometric compounds are very rare, with the notable exceptions like Gd$_5$Ge$_4$, doped CeFe$_2$ [1,2], and Nd$_7$Rh$_3$. In this article we address this issue further on the intermetallic compound Nd$_7$Rh$_3$. Recent magnetic studies on polycrystalline and single crystalline Nd$_7$Rh$_3$ indicate the existence of a magnetic-field-induced FOPT. There is so far, however, no proof from any microscopic technique proving electronic phase coexistence in Nd$_7$Rh$_3$ in the zero-field state following a field cycling across the first-order transition [3–5]. In the present work we investigate this issue using neutron diffraction (ND) data obtained in the presence of magnetic fields and at different temperatures.

II. EXPERIMENTAL DETAILS

Neutron diffraction data presented in this article were taken on polycrystalline samples of arc-melted Nd$_7$Rh$_3$. The synthesis conditions for the sample were similar to those reported earlier [3,4]. Magnetic characterizations have been carried out on a Quantum Design PPMS vibrating sample magnetometer (VSM). ND experiments were carried out on finely ground powder of Nd$_7$Rh$_3$ ingot on D1B and D2B diffractometers at Institute Laue Langevin (ILL), Grenoble, France. The ND patterns were also measured on E6 at Helmholtz-Zentrum Berlin (HZB), Berlin using the CHUF (cooling and heating in unequal field) protocol [5,6]. The sample was first cooled in zero field from 80 to 2 K, and

ND patterns were recorded at selected temperatures between 2 and 50 K in warming cycle under different fields, $H = 0$, 1.5, 2, 4, and 30 kOe. The same set of experiment was repeated after cooling the sample in a field of 30 kOe.

The powdered sample was packed in a vanadium container. Application of an external magnetic field might cause re-orientation of the ferromagnetic grains along the easy axis, and, therefore, to avoid this experimental artifact, a deuterated methanol-ethanol mixture was added to the sample at room temperature. This mixture, when cooled sufficiently rapidly, freezes in an amorphous state around 100 K and helps to lock the sample grains in a random manner to prevent any preferential orientation under magnetic field and does not contribute to any Bragg peak in the diffraction pattern, except for a hump at low angles.

III. RESULTS AND DISCUSSIONS

A. Magnetization measurements

In Fig. 1 the magnetization data of the Nd$_7$Rh$_3$ sample is shown, which is qualitatively in agreement with the previous reports [3,4]. For the zero-field-cooled (ZFC) state of the sample, the M versus T curve clearly reveals two peaks, one at $T_{N1} = 32$ K and another at $T_{N2} = 16$ K. For the case of the field-cooled (FC) state of the sample, T_{N1} corresponds to that of the ZFC case. However, there is a prominent difference in the vicinity of T_{N2}; below 16 K, M increases gradually with decreasing temperature, with a tendency towards saturation below T_{N2}.

B. Zero field neutron diffraction studies

In a previous ND work on Nd$_7$Rh$_3$ [7] measured on diffractometers PD-3 at Dhruva, Trombay and E6 and E9 at HZB, Berlin, no intense antiferromagnetic (AF) peak as seen in isostructural compounds such as Nd$_7$Ni$_3$, Er$_7$Rh$_3$, etc. at low Q ($= 4\pi \sin\theta / \lambda$) values [8–13] was observed and it was concluded that Nd$_7$Rh$_3$ is ferromagnetic at low temperatures. The surprising result that the magnetic structure of Nd$_7$Rh$_3$ should be different from its isostructural counterparts and the

*sudhindra@csr.res.in
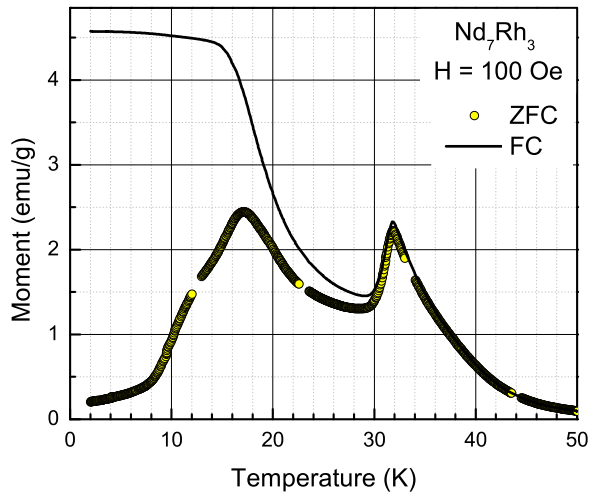
FIG. 1. (Color online) Magnetic susceptibility of Nd_7Rh_3 in an applied field of 100 Oe measured in zero-field-cooled (ZFC) and field-cooled (FC) state of the sample. The two magnetic transitions at 32 and 16 K are clearly seen from the figure.

relatively low magnetic moment values found at 2 K made us believe that a new experiment going to extremely low Q values should be attempted. A special arrangement of collimators and direct-beam stop enabled measurement of data on D1B and E6 from $Q = 0.027$ Å^{-1}, without any major interference from the direct beam.

In Fig. 2 the neutron diffraction patterns recorded at 1 K intervals from 2 to 50 K, across the two magnetic transitions, are shown. The ND patterns shown here were recorded on D1B using a wavelength of 2.52 Å. As the temperature is lowered to 32 K, a strong Bragg peak develops around $2\theta = 2.32^o$ (or $Q = 0.1$ Å^{-1}), which reaches a maximum around 16 K. Interestingly, the peak intensity decreases between 16 and 10 K, and again rises as T approaches 2 K but to a much lower intensity than at 16 K (~ 0.5 times). Comparing this with the
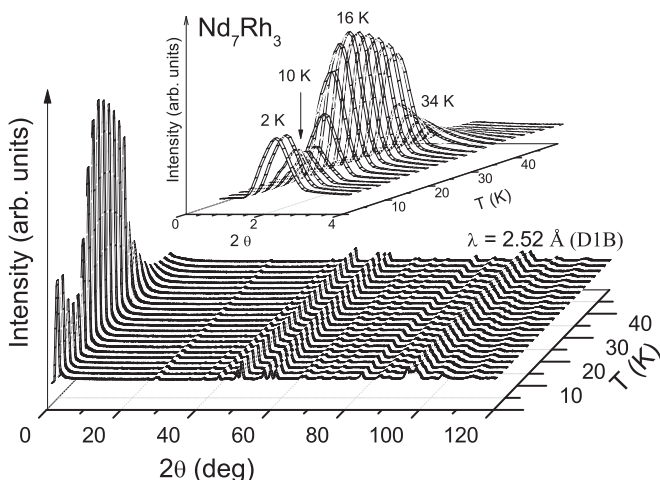
FIG. 2. Thermodiffractogram for Nd_7Rh_3 measured in the zero applied dc field is shown here. The inset exhibits the expanded region of the strong antiferromagnetic peak observed at a Q value (in 2θ) of 0.1 Å^{-1} (2.3^o).

data for Nd_7Ni_3, it is clear that this is the antiferromagnetic peak that eluded us in the previous measurements on the Nd_7Rh_3 compound [7]. The fact that it occurs at such a low Q (~ 0.1 Å^{-1}) indicates the magnetic cell to be much larger than the crystallographic unit cell. The d spacing of this dominant magnetic peak corresponds to ~ 60 Å in case of Nd_7Rh_3, whereas it is about 20 Å in case of the isostructural counterparts. All the ND patterns were refined by the Rietveld refinement method using FULLPROF suite programs [14,15]. For refining the crystallographic (nuclear) structure, ND patterns were recorded on D2B at ILL using a wavelength of 1.594 Å at selected temperatures 2, 10, 20, 50 K, and at room temperature.

Nd_7Rh_3 crystallizes in the space group $P6_3mc$ with Rh on the Wyckoff position $6c$ ($x \approx 0.188$). Nd occupies three nonequivalent crystallographic positions with Nd1 on $6c$ ($x \approx 0.54$), Nd2 on $6c$ ($x \approx 0.88$), and Nd3 on $2a$ ($z \approx 0.31$) [16]. First refinement was carried out in the paramagnetic state using data taken at about 50 K in order to ascertain the crystal structure [Fig. 3(a)]. Using the program K-Search, which is part of the FULLPROF suite of programs, the incommensurate propagation vector $\kappa_1 = [0\,0 \pm 0.100\,(1)]$ was obtained from the first magnetic peak. It was found to satisfy the Bragg conditions for all antiferromagnetic (AF) peaks at all temperatures and fields, e.g., the value of κ did not show any temperature or field dependence. Magnetic symmetry analysis using the program *BasIreps* was used to obtain the irreducible representations (IR) and their basis vectors (BV) for the magnetic atoms on the $6c$ (Nd1, Nd2) and $2a$ (Nd3) sites for $\kappa_1 = [0\,0\,\delta]$ [17,18]. There are six IRs for the site $6c$ and four IRs for the site $2a$; see Table I of the Supplemental Material [19]. Testing the different IRs using data taken at 20 K, e.g., below T_{N1} but above T_{N2}, it turned out that only IR3 of the $6c$ site and IR6 of the $2a$ site create intensity for the dominant $(0\,0\,0)^{\pm}$ peak at low angles. A very good refinement [Fig. 3(b), $R_{Mag} = 3.8\%$] was achieved using BV1 and BV2 of IR3 for Nd1/Nd2 and BV1 and BV2 of IR6 for Nd3. It was possible to force Nd1 and Nd2 to adopt the same coefficients and furthermore, to constrain for both sites BV1 = BV2—limiting thereby the magnetic moment related free parameters to only two—without degrading the refinement. The resulting magnetic structure [Fig. 4(a)] represents a sine-wave modulation in direction of the c axis with the magnetic moments within the hexagonal basal plane. The amplitudes were refined to 2.7 (3) μ_B on the Nd1/Nd2 sites and to 2.9 (3) μ_B on the Nd3 site. It is not possible to refine the data using a helical model as proposed in [11] for Ho_7Rh_3 where, however, no refinement of intensities had been attempted.

The change of the magnetic structure below T_{N2} leads to a decrease of the AF peaks and simultaneously to the increase of some nuclear Bragg peaks pointing to the appearance of a second magnetic propagation vector $\kappa_2 = [0\,0\,0]$. Using again the program *BasIreps*, the IRs and their BVs were determined for this κ_2; see Table II of the Supplemental Material [19]. No combination of the allowed six IRs for site $6c$ and the four IRs of site $2a$ were able to account satisfactorily for the additional magnetic Bragg intensity of the low temperature data. The best refinements ($R_{Mag} \approx 14\%$) were still obtained if IR6 of site $2a$ (Nd3) which represents a ferromagnetic (F) alignment within the hexagonal basal plane is included. BV2 of IR2 of
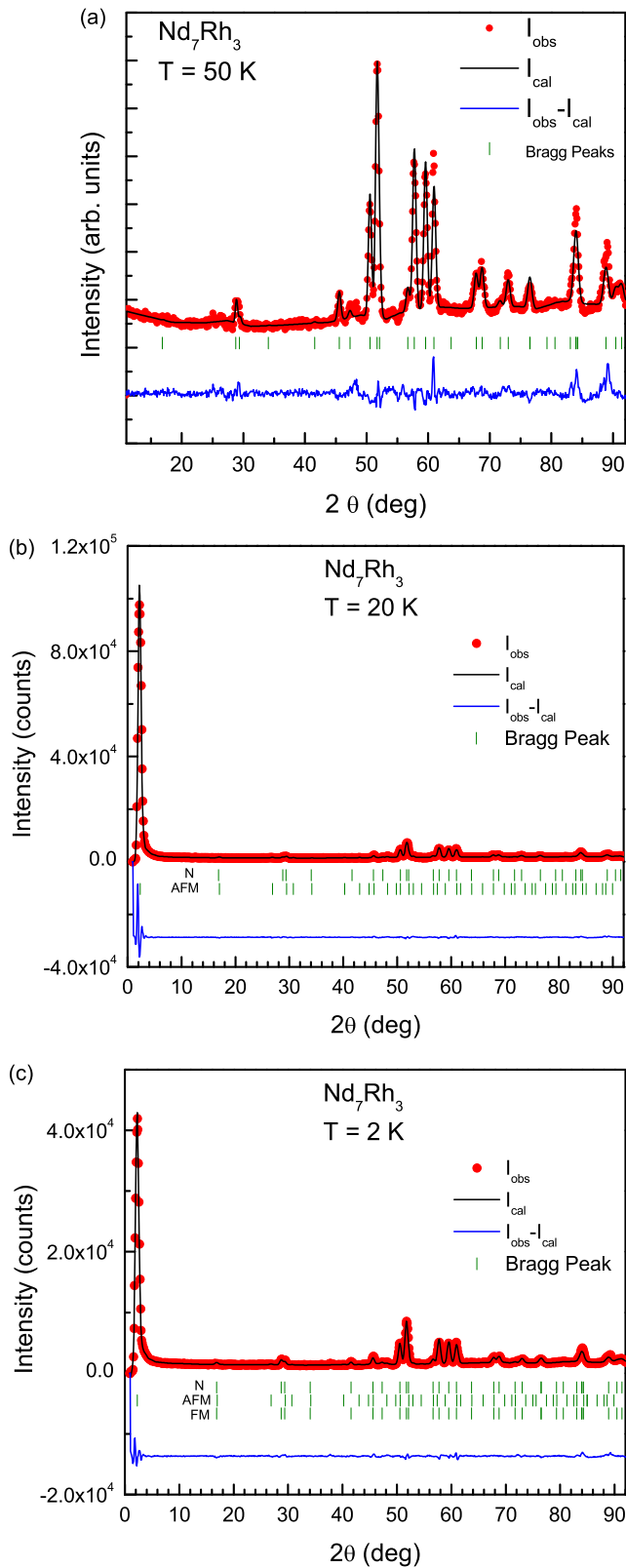
FIG. 3. (Color online) (a)–(c) Rietveld refinement of ND patterns recorded in zero field at T = 50, 20, and 2 K respectively, are shown here. The pattern at 2 K is refined using a structural phase (indicated by the first row of vertical tick marks), AFM phase (second row), and the FM phase (third row). Among the magnetic phases, at 20 K only the AFM phase exists, whereas at 50 K only the structural (nuclear) phase is refined.
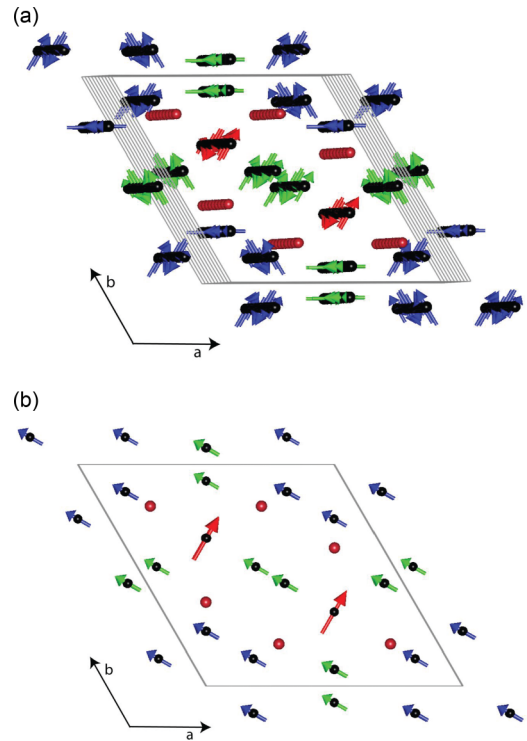
FIG. 4. (Color online) (a) Magnetic structure of the antiferromagnetic phase of Nd_7Rh_3 with Nd (Rh) atoms as black (red) balls shown in a slightly oblique view along the c axis. The sine-wave modulated moments are green (blue) for the Nd1 (Nd2) $6c$ sites and red for the Nd3 $2a$ site. (b) Magnetic structure of the ferromagnetic phase.

the $6c$ site allows as well an F coupling, however, only in c direction. Allowing the Nd2/Nd3 sites to adopt an F alignment within the hexagonal basal plane, a good refinement with only two magnetic moment related parameters again is obtained for the F phase ($R_{Mag} = 8.3\%$); Fig. 4(b) displays this magnetic structure. As both magnetic propagation vectors are present below T_{N2}, one has to discuss whether they act on the same sample volume or whether one is in the presence of a phase separation phenomena where different parts of the sample volume belong to the different magnetic structures. As long as the different magnetic structures cannot be linked to different crystallographic structures, it is not possible to ascertain directly a phase separation. The possibility of the phase separation scenario can be verified by attributing different scale factors in the Rietveld refinement—reflecting the phase percentage—to the two magnetic phases. The refinement of the data taken at T = 2 K shown in Fig. 3(c) was done assuming a separation into 36% AF and 64% F phase leading to magnetic moment values of $\mu_{Nd1/Nd2} = 3.1(2)\,\mu_B$ and $\mu_{Nd3} = 1.6(5)\,\mu_B$ for the AF phase and of $\mu_{Nd1/Nd2} = 1.7(1)\,\mu_B$ and $\mu_{Nd3} = 3.1(2)\,\mu_B$ for the F phase. These values do not contradict the phase separation scenario as the free ion moment of $\mu_{Nd3+} = 3.3\,\mu_B$.

In Fig. 5 the variation in the integrated intensity of the intense antiferromagnetic peak at $Q = 0.1\ \text{Å}^{-1}$, as a function of temperature, is shown. This figure also shows the influence of the external magnetic field on the intensity of the AFM peak. It can be clearly seen from the figure that, for the ZFC
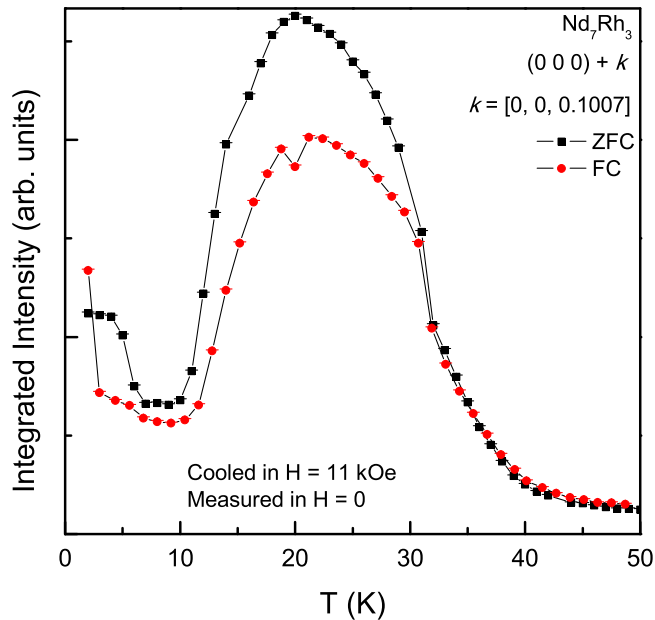
FIG. 5. (Color online) The figure shows a profile of the variation of the integrated intensity of the (0 0 0) magnetic peak qualitatively as a function of temperature to highlight the existence of a broad peak around 20 K. The same figure also shows the influence of cooling in the presence of external magnetic field (11 kOe) on the magnetic peak intensity. Both curves are obtained from measurements done in zero field while warming.

and FC states of the sample, the curves bifurcate drastically in the vicinity of T_{N1} (~32 K). Both the curves reach maxima around T_{N2} (~16 K). Below 16 K, the curves fall rapidly and reach a minimum around 10 K, and then show an upturn again below 7 K.

In order to follow the temperature dependent behavior of the AF and F components, a Rietveld refinement was done for data in the range 2–50 K. As it is not possible to determine the variation in the magnetic moment values and changing phase percentages simultaneously, these refinements were done using one fixed scale factor for the nuclear and the magnetic phases. In Fig. 6(a) the variation of cell volume as a function of temperature is plotted. There is only a marginal change in cell volume around the first transition temperature (T_{N1} ~ 32 K). A further, clearer anomaly is seen near the second transition temperature (T_{N2} ~ 16 K) as the temperature is lowered. Anomalies in cell parameters around magnetic transition temperatures are an indication of distortion in the crystal lattice due to quantum fluctuations arising due to coupling of magnetic and elastic degrees of freedom, as observed in some recent studies [20,21].

The variation of the AF and F magnetic moment values (Nd1 = Nd2 and Nd3) is shown in Fig. 6(b). The AF moments appear below T_{N1} = 32 K and increase down to T = 16 K where the F phase appears. Concomitant with the increase of the F component, the AF moment values decrease down to about 10 K. Below 10 K, the inverse effect is seen with AF (F) moments increasing (decreasing) slightly again. As the neutron data were measured during heating cycle, this behavior could
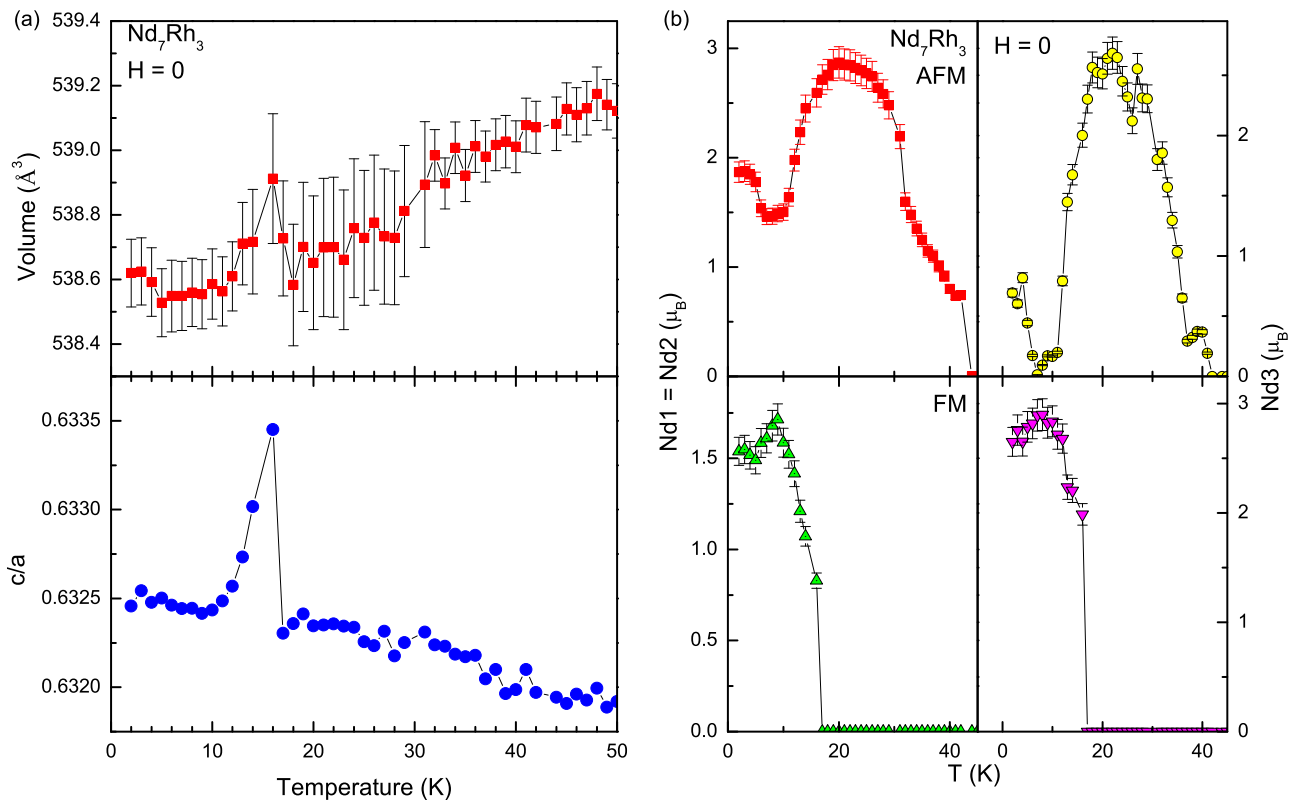
FIG. 6. (Color online) (a) Thermal variation of unit cell volume calculated from ND patterns recorded in zero field is shown here. The bottom panel highlights the variation in the *c/a* ratio. (b) The figure exhibits the site moments for Nd1 (=Nd2) and Nd3. The top and bottom panels indicate AFM and FM moments.

be linked within the phase separation scenario to a kinetic hindrance where due to a too fast cooling to 2 K, the phase equilibrium between F and AF phases had not been attained.

C. In-field neutron diffraction studies

We have also performed neutron diffraction measurements in the presence of magnetic fields in order to understand the anomalies following the field-induced first-order transition seen in magnetization data. We have chosen an upper limit of 11 kOe, since the critical field at which the field-induced first-order transition is observed at 2 K falls below this field, as inferred from the magnetization data [3,4,7]. ND experiments were carried out at 2 and 20 K at different applied magnetic fields between 0 and 11 kOe.

In Fig. 7(a) the influence of magnetic field on the (0 0 0) magnetic peak at $T = 2$ K is shown. Application of a magnetic field of 11 kOe completely suppresses the magnetic peak with a corresponding change in cell volume, as shown

in Fig. 7(c). In the ND measurement carried out immediately after removing the field, this magnetic peak does not reappear or return to its original state, indicating the arrest of the high-field magnetic state. Similar observations have been made in other systems exhibiting field-induced first-order transitions, such as charge ordered manganite $La_{0.5}Ca_{0.5}MnO_3$ and shape memory alloy $Ni_{37}Co_{11}Mn_{42.5}Sn_{9.5}$ [6]. However, this state is clearly different from the one just above T_{N2}. In Figs. 7(b) and 7(d) the influence of magnetic field on the magnetic state at 20 K is shown. In the ZFC state, the $(0\,0\,0)^{\pm}$ magnetic peak is clearly seen and its intensity at 20 K is higher by a factor of 2.5 than at 2 K. However, contrary to the behavior at 2 K, though the magnetic peak is completely suppressed by the application of magnetic field, the virgin peak reappears on removing the field. The arrest of the magnetic state observed at 2 K is thus absent at this temperature, which clearly shows that the devitrification of the arrested state under the applied field at this temperature is immediate on the removal of the field.
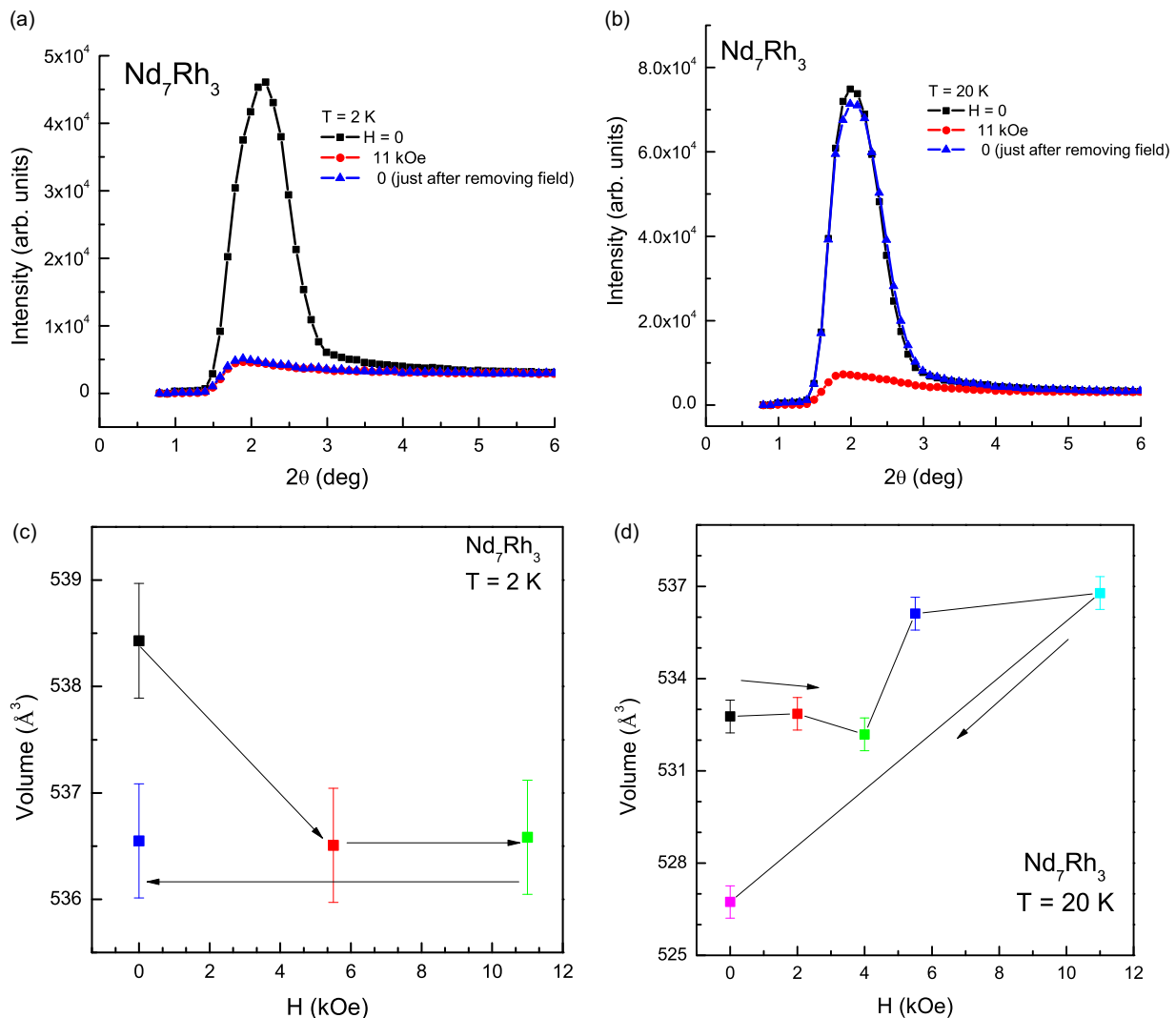
FIG. 7. (Color online) (a) ND patterns measured at 2 K in three conditions after zero field cooling the sample. In the first step ND patterns were measured in zero field, and then in 11 kOe, and finally in zero field immediately after removing the field. (b) ND patterns measured at 20 K again, in three conditions, that in $H = 0$, 11 kOe, and again in 0, immediately after removing the field. (c) and (d) Changes in the cell volume under the influence of the magnetic field at 2 and 20 K, respectively.
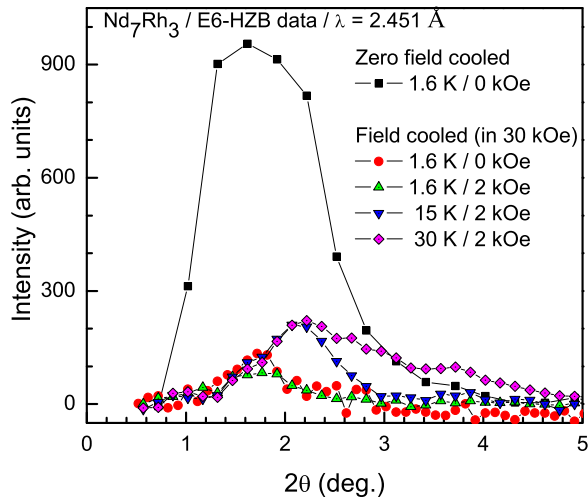
FIG. 8. (Color online) ND experiments were carried out on Nd_7Rh_3 after cooling the sample in one field ($H = 0$ or 30 kOe), and then measuring ND patterns in another field ($H = 0$ or 2 kOe) following the CHUF (cooling and heating in unequal fields) protocol.

In order to probe the in-field neutron diffraction data further, we focused on measuring ND patterns as a function of temperature after cooling the sample in a certain field, and then measuring ND patterns at selected temperatures while warming the sample in a different field. The choice of cooling field was 30 kOe, so that the transformation from antiferromagnetic to ferromagnetic state, as per magnetization curves, is complete. ND was measured at several selected temperatures between 1.6 and 50 K in different warming magnetic fields. These ND experiments were carried out on E6 at HZB, and focus was in the Q range of 0.02–0.7 Å^{-1} (in terms of degrees, between 0.6 and 5 deg in 2θ). In Fig. 8 the influence of cooling and heating in unequal fields can be clearly seen. When the sample is cooled in zero field to 1.6 K, and ND pattern measured in zero field, a strong but very broad magnetic peak centered at $Q \sim 0.1$ Å^{-1} is observed. In the next cycle, the sample was cooled from 100 to 1.6 K in a field of 30 kOe and as expected, the $(0\,0\,0)^\pm$ peak at 0.1 Å^{-1} was completely suppressed. At this

temperature, the field was then reduced to 2 kOe and the ND pattern measured. It is observed that while the magnetic peak at 0.1 Å^{-1} remains completely arrested, a small hump appears at $Q \sim 0.07$ Å^{-1}. On warming the sample in the applied field of 2 kOe, the $(0\,0\,0)^\pm$ peak at 0.1 Å^{-1} reappears with a much smaller intensity at 15 and 30 K, indicating a partial devitrification of the arrested state. However, the hump at $Q \sim 0.07$ Å^{-1} remains clearly evident, indicating the possibility of another underlying magnetic order not as dominant as the one at $Q \sim 0.1$ Å^{-1}. Hence, in-field neutron diffraction measurements using the CHUF protocol throw up some interesting possibilities of manipulating magnetic order. Detailed experiments on single crystalline Nd_7Rh_3 may be desirable to understand the field-induced changes to the magnetic structure and their implications on magnetism of this compound.

IV. CONCLUSIONS

Coexistence of antiferromagnetism and ferromagnetism has been shown microscopically using neutron diffraction experiments in Nd_7Rh_3 below the second ordering temperature (T_{N2}). Between T_{N1} and T_{N2} antiferromagnetism has been observed. A strong anomaly has been observed in the unit cell volume around T_{N2}, attributable to a strong spin-lattice coupling. Application of magnetic field also results in observable compression of the cell volume. Neutron diffraction patterns measured using the CHUF protocol provide microscopic evidence for a partial arrest of the high-field magnetic state following field-induced transition at 2 K, thus offering direct evidence for phase coexistence in a stoichiometric compound.

[1] M. K. Chattopadhyay, M. A. Manekar, A. O. Pecharsky, V. K. Pecharsky, K. A. Gschneidner, Jr., J. Moore, G. K. Perkins, Y. V. Bugoslavsky, S. B. Roy, P. Chaddah, and L. F. Cohen, Phys. Rev. B **70**, 214421 (2004).

[2] E. Dagotto, T. Hotta, and A. More, Phys. Rep. **344**, 1 (2001).

[3] K. Sengupta and E. V. Sampathkumaran, Phys. Rev. B **73**, 020406 (2006).

[4] K. Sengupta and E. V. Sampathkumaran, J. Phys.: Condens. Mater **18**, L401 (2006).

[5] A. Banerjee, K. Kumar, and P. Chaddah, J. Phys.: Condens. Mater **21**, 026002 (2009).

[6] V. Siruguri, P. D. Babu, S. D. Kaushik, A. Biswas, S. K. Sarkar, M. Krishnan, and P. Chaddah, J. Phys.: Condens. Mater **25**, 496011 (2013).

[7] S. Rayaprol, V. Siruguri, A. Hoser, P. Henry, and E. V. Sampathkumaran, J. Phys. Conf. Ser. **340**, 012064 (2012).

[8] A. Tanaka, T. Tsutaoka, and T. Shigeoka, Physica B **403**, 3248 (2008).

[9] T. Tsutaoka, Y. Andoh, S. Kawano, G. Nakamoto, D. T. K. Ahn, M. Kurisu, and T. Tokunaga, J. Alloys Compd **408-412**, 181 (2006).

[10] T. Tsutaoka, Y. Nakamori, T. Tokunaga, and Y. Itoh, J. Phys. Soc. Jpn. **70**, 199 (2001).

[11] T. Tsutaoka, Y. Nishiume, T. Tokunaga, Y. Nakamori, Y. Andoh, S. Kawano, G. Nakamoto, and M. Kurisu, Physica B **327**, 352 (2003).

[12] T. Tsutaoka, A. Tanaka, Y. Andoh, S. Kawano, M. Kurisu, and G. Nakamoto, Physica B **385-386**, 353 (2006).

[13] X. Xu, S. Kawano, T. Tsutaoka, Y. Andoh, M. Kurisu, G. Nakamoto, Y. Nakamori, T. Tokunaga and H. Kadomatsu, J. Phys. Chem. Solids **60**, 1209 (1999).

[14] H. M. Rietveld, J. Appl. Crystallogr. **2**, 65 (1969).

[15] J. Rodriguez-Carvajal, Physica B **192**, 55 (1993).

[16] J. V. Florio, N. C. Baenziger, and R. E. Rundle, Acta Crystallogr. **9**, 367 (1956); and Landolt-Börnstein III/43A4 Index of structures, space groups (186).

[17] J. Rodriguez-Carvajal, BASIREPS: A program for calculating irreducible representations of space groups and basis functions for axial and polar vector properties Part of the FULLPROF suite of programs available at http://www.ill.eu/sites/fullprof/.

[18] C. Ritter, Solid State Phenom. **170**, 263 (2011).

[19] See Supplemental Material at http://link.aps.org/supplemental/10.1103/PhysRevB.90.134417 for the tables in the summary file describes the Irreducible representations (IR) and their basis vectors (BV) for propogation vector $k1 = (00\delta)$ and $k_2 = (000)$ for Wyckoff sites for 6c and 2a in space group $P6_3mc$.

[20] I. Paul, Phys. Rev. Lett. **107**, 047004 (2011).

[21] S. Chi, F. Ye, P. Dai, J. A. Fernandez-Baca, Q. Huang, J. W. Lynn, E. W. Plummer, R. Mathieu, Y. Kaneko, and Y. Tokura, Proc. Natl. Acad. Sci. USA **104**, 10796 (2007).